Research Article

Numerical investigation of free rotor aerodynamics

Sarih SARI[1],* , **Ali DOĞRUL[2]** , **Seyfettin BAYRAKTAR[3]**

[1]Department of Naval Architecture and Marine Engineering, Yildiz Technical University, İstanbul, 34349, Türkiye
[2]Department of Naval Architecture and Marine Engineering, Turkish Naval Academy, National Defence University, İstanbul, 34334, Türkiye
[3]Department of Marine Engineering Operations, Yildiz Technical University, İstanbul, 34220, Türkiye

ARTICLE INFO

ABSTRACT

Rotor aerodynamics is important for rotary-wing aircraft especially those located in naval surface combatants. The aerodynamic interaction between the helicopter, its rotor and the ship structure should be investigated precisely. This study focuses on the aerodynamic performance of four-blade rotor geometry of Sikorsky S-76 helicopter. The main rotor geometry was analyzed numerically in the free condition in an unbounded flow domain. Unsteady Reynolds-Averaged Navier-Stokes (URANS) equations in rigid body motion (RBM) on unstructured grids were solved by discretizing the computational domain with finite volume elements and using the Shear-Stress Transport (SST) k-ω turbulence model. The numerical approach was verified using the GCI method and validated with the relevant data available in the literature. It was found that in hover condition, non-dimensional thrust and the torque coefficients change slightly with the rotation speed of the rotor due to possibly the collective pitch angle. However, whereas the torque coefficient varies slightly with rotor speed, the thrust coefficient fluctuates substantially.

Cite this article as: Sarı S, Doğrul A, Bayraktar S. Numerical investigation of free rotor aerodynamics. Sigma J Eng Nat Sci 2024;42(6):1826–1837.

INTRODUCTION

Ship aerodynamics is a crucial research area that combines naval architecture and aerospace engineering. Given the ship's large superstructure, which includes electronic devices, radars, weapon systems and masts, understanding the airflow around it becomes significant for the fixed/rotary wing aircraft operating within the ship's airwake. This brings to light the interaction between the ship, the helicopter, and its rotor. In this regard, several studies can be found in the open literature enlightening the rotor aerodynamics and its interaction with the ship superstructure.

Such studies can traditionally be performed by three different approaches: experimental, numerical, and on-site studies. The latter one includes the recovery maneuvers by the pilots during the take-off and landing operations while experimental studies are performed in wind tunnels and/or towing tanks with scaled models. Finally, numerical studies leverage computational fluid dynamics (CFD), wherein governing flow equations are solved utilizing models representing helicopter-ship dynamic interference or a hovering main rotor operating near ship structures [1].

***Corresponding author.**
*E-mail address: sarih@yildiz.edu.tr

This paper was recommended for publication in revised form by
Editor-in-Chief Ahmet Selim Dalkilic

For helicopter operations, the hovering capability is of paramount importance, and it also imposes constraints on design, particularly in terms of power requirements. Aerodynamics theorists have proposed several wake models to predict hover performance such as one-dimensional (1D) momentum theory or disc actuator theory, blade element momentum theory, BEMT (an improved version of the 1D momentum theory), dynamic-inflow (finite-state) model, prescribed-wake model, free-wake model. The latest advancements have led to the implementation of an improved model known as the wake-capturing model, which serves as a high-fidelity computational fluid dynamics (CFD) method [2].

The ship-helicopter interaction during the hovering was investigated numerically by Wakefield et al. [3] for the helicopter rotor. Only the main rotor of Westland Lynx aircraft was considered. The rotor was located over the center point of the flight deck of the generic ship called Simple Frigate Ship (SFS) under the wind speed of 40 knots. The studies were performed for the headwind, the wind approaching from a beam of the ship on the starboard side at 90°. The studies proved that CFD solutions are generally able to predict large-scale flow phenomena. Lee and Zan [4] investigated the interaction of the rotor and ship experimentally. Canadian Patrol Frigate and CH-124 helicopter fuselage were used, and the rotor of the helicopter was located at different hover positions. Interaction that results from complex flow field between the main rotor wake and the fuselage of a model helicopter was experimentally investigated by Gregorio et al. [5] with the aid of Particle Image Velocimetry (PIV) in a low-speed wind tunnel. They considered the isolated ONERA 7AD fuselage with a rotating hub without blades and the fully equipped helicopter model with a four-bladed rotor for a wide range of mission envelopes. All tests were done with a constant rotor speed of 956 rpm (revolution per minute). It was shown that the rotor wake has a strong influence on the fuselage and its drag. Different wind angles were investigated and a wind envelope was obtained. In the study of Barakos et al. [6], rotor effects were investigated numerically using the Canadian Patrol Boat (CPB). When the actuator disc method was used, coupling effects were observed in the positions where the rotor was close to the ship. These effects do not appear in the superposition method. Results compared with experimental data showed that rotor loads vary between close-to-deck flight and forward flight. In another study [7], the authors performed numerical calculations to determine the helicopter rotor effects for the Canadian Patrol Frigate. By solving the Navier-Stokes equations using the actuator disk method, the airwake around the helicopter and rotor was simulated. As a result, it was shown that different air loads can occur on the helicopter fuselage close to the deck. Jain and Potsdam [8] focused on the validation of the S-76 model-scale rotor through Computational Fluid Dynamics (CFD) using the HPCMP CREATETM-AV Helios software suite. High-resolution, time-accurate simulations were conducted for various collective angles and two different tip Mach numbers. The obtained results, encompassing performance, air loads, and tip-vortex trajectory data, were compared to test measurements. Excellent agreement was observed for the entire range of collective angles studied. In a thesis work [9], the author investigated the airwake flow problem for the SFS2 model using RANS and Large Eddy Simulation (LES) solver. The ship model was simulated in different positions using the ship motion data of similar-sized ships available in the literature. Following this, the helicopter rotor effect was simulated with an actuator disc for different deck inclination angles. Perera et al. [10] studied the aerodynamics of the helicopter rotor of Bell 212 helicopter consisting of a 2-blade NACA 0012 airfoil profile. The study was carried out in three stages. Hover, vertical and forward flight conditions were analyzed by the blade element method and momentum theory. SST k-epsilon was used as the turbulence model in the study. Shi et al. [11] focused on the numerical investigation of a helicopter landing on a shipboard. They used two methods for modeling rotor effects. First, the steady rotor model (SRM) based on the momentum source approach was utilized. The other model is the unsteady rotor model, which is derived from the moving overset mesh. It was observed that both models can capture complex interactions well. Sahbaz et al. [12] investigated the effects of ground effect on helicopter performance. It is demonstrated experimentally and numerically that the same thrust can be obtained with lower power consumption by changing the flow thrust value from the ground to the blades. In addition, the study was repeated using rotating ground. The rotating floor eliminated the advantages of the ground effect and created a chaotic structure. As a result of the movement of the ground, unsymmetrical vortexes were formed. This was shown to be risky for helicopter operations. Abras et al. [13] analyzed the effects of the mesh algorithm on the hover condition using the S-76 main rotor. Also, the effects of the rotor hub on the performance were investigated. It was reported that the effect of hub-induced effects is small and the blade tip grid refinement and leading edge and trailing edge grid refinement have greater effects on the results. In the study of Tan et al. [14], blade aerodynamics and unsteady air loads for a tandem rotor of a CH-46 helicopter were numerically investigated using the panel method. Surface effects were calculated on the model scale Landing Helicopter Assault (LHA) ship. The results were compared with the experimental results of NASA Ames Research Center. It was discovered that the vertical velocities determined by numerical calculations matched those of the experiments. Kara et al. [15] investigated time step size and sub-iterations on the integrated parameters for a four-bladed Sikorsky S-76 rotor by higher order Galerkin off-body discretization method to solve flow equations on unstructured meshes. The numerical studies were performed for the Reynolds number based on the reference chord (Re=1.2×10^6), the tip Mach number of Ma=0.65 and the rotations of $1/2^0$, $1/4^0$ and $1/10^0$. It

was found that smaller time steps speed up the convergence rates however, the thrust coefficient does not change considerably with time steps. In their study, Barakos et al. [16] discussed the rotor wakes using the rotor momentum theory. Three-dimensional (3D) load effects and tip losses were determined by the actuator disc method. Numerical studies using the SST k-ω model were performed for fully turbulent flow. As a result of numerical studies with the actuator disk, the vortex structures around the rotor disk were modeled precisely. The study of Bardera et al. [17] focused on the helicopter rotor-ship interaction experimentally. PIV measurements were obtained for various scenarios by mimicking the rotor effect of a Sea King navy helicopter on a frigate. The helicopter rotor was placed in different positions to investigate the ground effect on the helicopter's performance. Ibacoglu and Arikoglu [18] developed a new methodology for main rotor blades and investigated their performance and structural characteristics by considering several parameters. They validated their numerical and experimental data with the test results of Sikorsky UH-60 and S-76 helicopters for hover and forward flight conditions at 750 constant rpm. Upon good agreement, it was shown that by means of the developed methodology thousands of concepts can be evaluated in a very short time. Effect of blade tip shape of four-bladed and Mach scaled Sikorsky S-76 in hover condition was studied in terms of rotor performance, blade airloads, tip-vortex strength and positions [2]. They tested Spalart-Allmaras and SST k-omega turbulence models and implied that both are consistent with the experimental data at all thrust levels.

This study is centered on the numerical investigation of helicopter rotor aerodynamics in free conditions. Unlike fixed-wing aircraft, helicopters are more intricate, relying on a single component known as the rotor for lift, thrust, and control [18]. Consequently, understanding rotor aerodynamics is paramount. In this context, a Sikorsky S-76 four bladed rotor geometry was used. The rotor was analyzed in hover conditions at various rotor velocities and one headwind (40 knots) wind velocity, crucial for maneuvers involving descending and suspending. Numerical analyses were conducted using commercial CFD software with URANS equations as governing equations. The numerical uncertainty was determined using the GCI method with respect to grid size. Rotor parameters were acquired at different advance ratios of the rotor blade and 40 knots relative wind velocity, and results were validated for hover conditions at maximum rotor revolution using available data from the literature. Finally, the numerical results were discussed in terms of rotor rpm versus non-dimensional thrust force, providing detailed insights into the effects of varying rotor and wind velocities.

In some rotor aerodynamic studies, it is seen that the interaction between ship and rotor is frequently analysed. Ashok and Rauleder investigated the complex aerodynamic interactions between the rotor and ship airwakes during the landing of rotorcraft on ship decks. Conventional simulations of one-way couplings, in which the rotor reacts to the ship's airwake but not the other way around, may overlook important events, particularly when the ship is moving. This work used a Graphics Processing Unit (GPU) accelerated Lattice–Boltzmann Method for one- and two-way coupled ship–rotorcraft interactional simulations, using the NATO Generic Destroyer as a model. The results demonstrated clear frequency profiles and differences in closed-loop pilot response between one-way and two-way coupling schemes, and they agreed well with wind tunnel measurements [19]. Fernandez et al. examined the unstable aerodynamic loading on a helicopter within the airwake of a typical destroyer undergoing different ship motions. The study takes into account several modeling methodologies and finds very slight variations in helicopter loads among various motion kinds. Nevertheless, in instant load and air-velocity spectra as well as RMS (root mean square) loads, the effects of ship motion are particularly noticeable. Thrust load spectra show dominant peaks and harmonics at the ship motion frequency, especially in normal 2-DOF(degree of freedom) ship motions and sinusoidal pitching. These results elucidate the links between ship airwake and helicopter loading and their effects for flight operations, offering fundamental insights into the interplay between the turning rotor and the moving ship[20].In order to study the aeroelasticity of a rotor in shipboard helicopter operations, Yu et al. developed a loose coupling model for computational fluid dynamics and computational structural dynamics (CFD/CSD). This model uses a CFD solver based on Reynolds-averaged Navier-Stokes (RANS) equations and a CSD solver based on the moderate deflection beam model to predict the aeroelastic behavior of the rotor during engagement and disengagement with ship motions. The efficiency of the simulation is verified through comparison with experimental data. According to the analysis, elastic deflection has a substantial effect on the aerodynamic forces of the blades under certain wind-over-deck situations. Increasing wind direction and angles may result in considerable negative elastic twist deflection, which increases the possibility of a decline in aerodynamic forces and possible over deflection [21]. Zamiri and Chung aimed to explore the impact of wind direction and the bow section of a ship on turbulent flow characteristics in the airwake during shipboard operations, employing delayed detached eddy simulation (DDES). Numerical simulations were conducted with two ship models, Simple Frigate Shapes 1 and 2 (SPF1 and SFS2), at a scale of 1:12.5, considering seven wind direction angles. The DDES results were validated against experimental data from Kulite pressure sensors and Particle Image Velocimetry (PIV) sensors at various ship deck locations. The findings indicated minimal influence of the ship's bow on both the airwake flow and deck flow-field. However, an increase in wind direction angles correlated with elevated turbulent kinetic energy, heightened asymmetry in the flow-field, and increased pressure fluctuations

and unsteadiness over the ship deck, underscoring the significance of these factors in shipboard operations [22].

COMPUTATIONAL METHOD

This paper specifically delves into the rotational behavior of a helicopter rotor equipped with four blades under hover and headwind conditions. Hovering, a crucial phase preceding a helicopter's landing on the ship's flight deck, entails maintaining a constant position. During this phase, the lift and thrust generated by the rotor system counteract the weight and drag forces acting in the opposite direction. In addition to this, a headwind condition was considered as 40 knots considering the effects of the ship and wind together.

In the current work, it is assumed that the rotor is fully rigid and isolated, and it is hovering out-of-ground. The numerical setup consists of the computational domain, boundary conditions, grid generation and physics modeling. The details of each process are given below.

Rotor Geometry

The rotating rotor under investigation in the present study is the one used on the Sikorsky S-76 helicopter. The Sikorsky S-76 is a medium-sized helicopter suitable for marine operations and hence used by many navies. Table 1 gives some of the features of the rotor used on Sikorsky S-76. The 3D CAD (computer-aided design) model generated using the data extracted from the report [23] is given in Figure 1. As stated in Table 1, the rotor blades use SC1013R8, SC1095R8 and SC10954 airfoils.

The rotor used on the Sikorsky S-76 consists of four blades with a blade radius of 6.7056 m. The full-scale model

Table 1. S-76 main rotor particulars [23], with permission from Frontiers

Parameter	Value
Rotor diameter (m)	13.4112
Rotor solidity	0.0748
Number of blades	4
Airfoil sections	SC1013R8, SC1095R8, SC10954
Rotor area (m²)	141.262
Rotor velocity (RPM) (100%)	293
Rotor tip velocity (m/s) (100%)	205.747

of the rotor was used in the present study. As shown in Figure 1, the rotor tip was taken as rectangular.

Governing Equations

The numerical analyses were conducted using commercial CFD software Star CCM+ developed by Siemens PLM to solve URANS equations. The governing equations are the continuity and the momentum equations [24,25] considering the flow is unsteady, incompressible and turbulent. The continuity equation can be given as:

$$\frac{\partial U_i}{\partial x_i} = 0 \tag{1}$$

The mean momentum equations can be written in tensor notation and Cartesian coordinates.

$$\frac{\partial U_i}{\partial t} + U_j \frac{\partial U_i}{\partial x_j} = -\frac{1}{\rho}\frac{\partial P}{\partial x_i} + \frac{\partial}{\partial x_j}\left[\nu\left(\frac{\partial U_i}{\partial x_j} + \frac{\partial U_j}{\partial x_i}\right)\right] - \frac{\partial \overline{u_i' u_j'}}{\partial x_j} \tag{2}$$
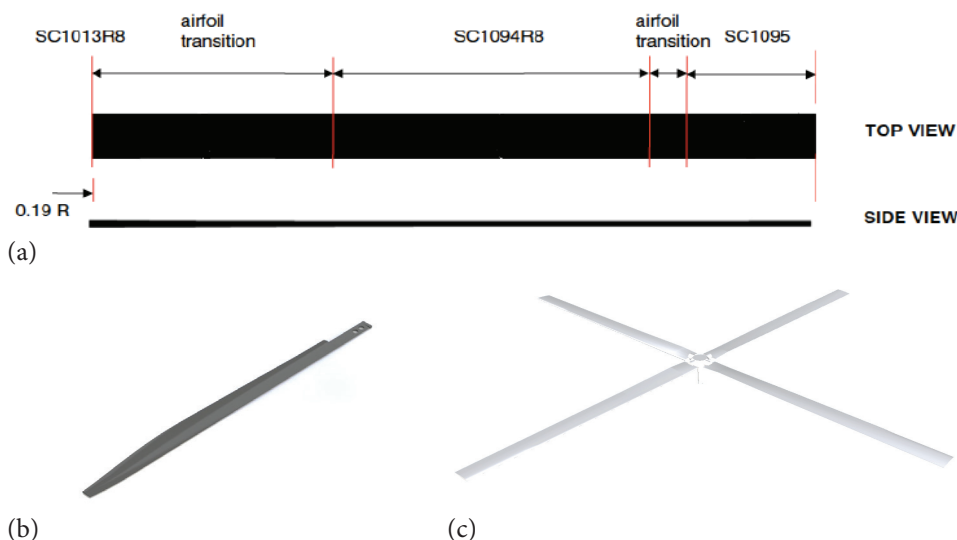

(a)

(b)   (c)

Figure 1. The rotor blade airfoil and chord distributions from [2] (a), 3D view of one blade (b) and rotor configuration (c) of Sikorsky S-76.

Here, ρ depicts the fluid density, kg/m³; U_i is the velocity, m/s; P represents the pressure, Pa; v is the kinematic viscosity, m²/s. The last two terms belong to the viscous stress tensor and Reynolds stress tensor, respectively. The details about Reynolds stress tensor (i.e., $\overline{u'_i u'_j}$ can be found in the studies of Wilcox in detail [26,27]. The numerical study performed by [2] compares the performance of both Spalart-Allmaras (SA) and shear stress-transport (SST) k-omega study reveals that both SA and SST k-omega can compute accurately the thrust generated by the rotor blades used in Sikorsky S-76. Hence, the SST k-omega turbulence model was employed in the present study. The governing equations of the SST k-omega turbulence model are presented below.

$$\frac{\partial k}{\partial t} + U_j \frac{\partial_k}{\partial x_j} = \frac{\partial}{\partial x_j}\left[\left(v + \sigma^* \frac{k}{\omega}\right)\frac{\partial k}{\partial x_j}\right] + P_k - \beta^* k\omega \tag{3}$$

$$\frac{\partial \omega}{\partial t} + U_j \frac{\partial_k}{\partial x_j} = \frac{\partial}{\partial x_j}\left[\left(v + \sigma \frac{k}{\omega}\right)\frac{\partial \omega}{\partial x_j}\right] + \alpha \frac{\omega}{k} P_k + \beta \omega^2 + \frac{\sigma_d}{\omega}\frac{\partial k}{\partial x_j}\frac{\partial \omega}{\partial x_j} \tag{4}$$

Where P_k is the production rate of the turbulent kinetic energy and other parameters are the closure coefficients [26,27].

Mesh and Physics Modeling

The 4-bladed rotor was placed in two co-axial cylindrical domains in which the inner one is small while the outer cylinder is quite large as shown in Figure 2. Inspired by the approach used for open water propeller and ship self-propulsion analyses [28,29], the large outer region is kept motionless (static) while the small inner one is rotating with a predefined rotational velocity. Figure 2 shows the inner and outer cylinder domains non-dimensionalized with rotor diameter.
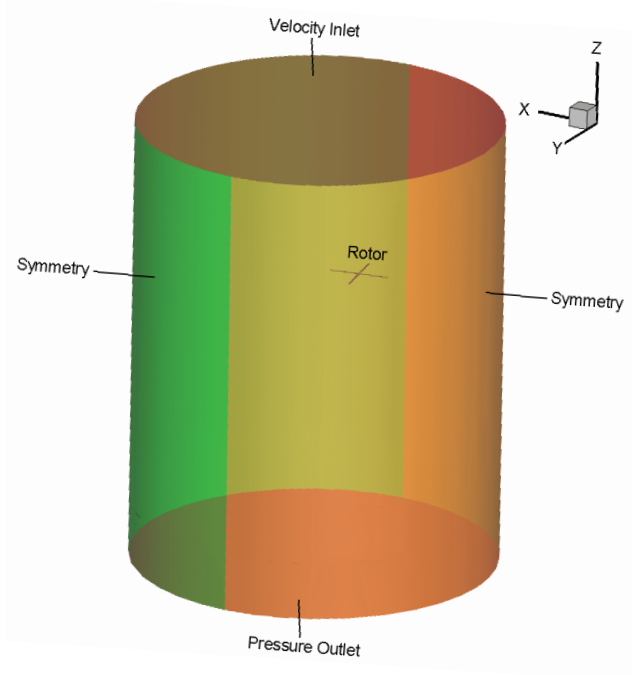
Figure 3. Boundary conditions applied on the surfaces

As given in Figure 3, the top surface of the computational domain is set as a velocity inlet while the bottom surface is defined as pressure outlet. The remaining outer surfaces of the domain is considered as symmetry. The rotor blades, the hub and the shaft surfaces are dictated to be wall that satisfies the no-slip boundary condition. As can be seen, the working domain is large enough to prevent any backflows.

The computational domain was discretized with finite-volume hexahedral elements. The trimmer mesh
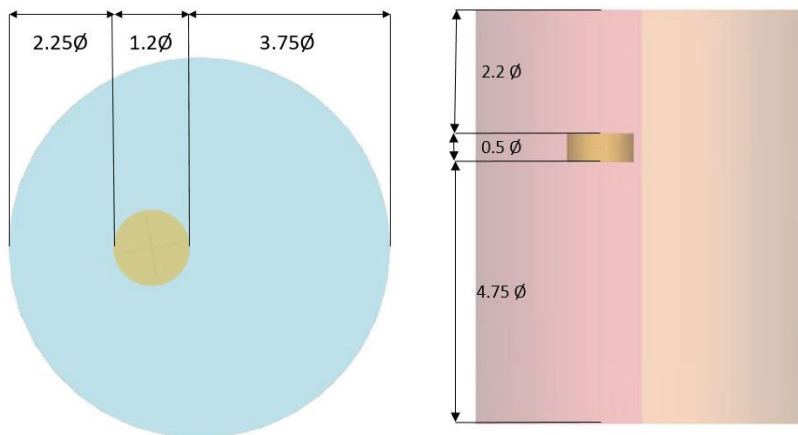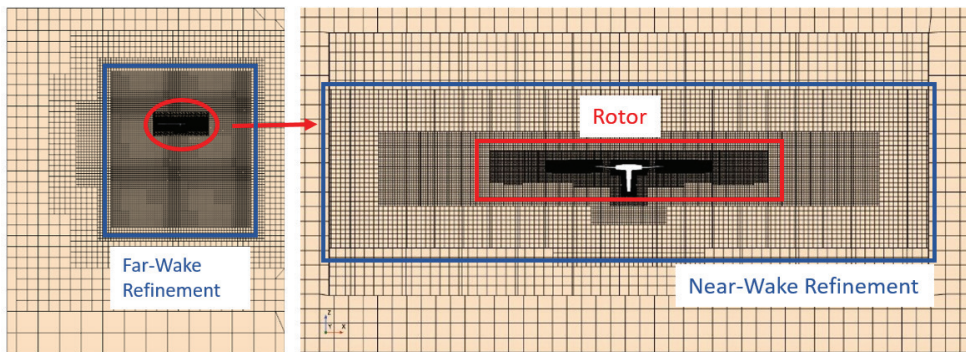
Figure 2. Domain dimensions.

Figure 4. Mesh structure of the computational domain.

algorithm provides a fully hexahedral grid structure. Local mesh refinements were utilized around the rotor blades and the rotating region. Figure 4 shows the mesh structure on the computational domain and local refinements around the rotating region.

Since the flow was considered 3D, turbulent and incompressible, the appropriate turbulence model (SST k-omega) was chosen and the unsteady RANS equation was solved in an unsteady manner. The time step size was calculated with the assumption that the rotor rotates 5^0 per time step. The Rigid Body Motion (RBM) approach was employed for the rotor rotation with a constant rotational velocity.

NUMERICAL RESULTS

Verification Study

The numerical analyses were conducted using a dense mesh algorithm and time step size. However, the numerical

Table 2. Grid numbers

Region	Fine	Medium	Coarse
Rotating	3441822	2259387	1292620
Static	1134939	430333	173233
Total	4576761	2689720	1465853

Table 3. Spatial uncertainty values for both cases

Parameter	Values for 0 knot	Values for 40 knot
N_{fine}	4576761	4576761
N_{medium}	2689720	2689720
N_{coarse}	1465853	1465853
$\emptyset_{fine}$ (N)	7020.00	33104.80
$\emptyset_{medium}$ (N)	6537.32	31558.07
$\emptyset_{coarse}$ (N)	6928.51	38552.59
U_N (%)	6.52	2.89

approach needs to be verified to determine the numerical uncertainty. In this study, the grid number was verified in terms of spatial uncertainty since the time step size was kept constant as the rotor is rotating 5 degrees per time step. The verification study was made for the rotor at hover condition, so the free stream velocity was considered as 0 knot. Following this, the uncertainty study was extended to headwind condition considering the velocity as 40 knot. The rotor was rotating at 293 rpm (100 % condition) for both conditions.

The numerical uncertainty was obtained using the well-known Grid Convergence Index (GCI) method. The method was based on Richardson extrapolation [30] and proposed by Celik et al. [31]. This method is widely used in ship hydrodynamics and aerodynamics studies [32,33] and suggested by AIAA [34]. Details of the GCI method can be found in Praveen et al. [32]. The uncertainty was checked whether it has a monotonic or oscillating convergence [35]. Table 2 shows the grid numbers of each grid spacing. Here, fine, medium, and coarse grid numbers were obtained by considering the refinement ratio as $\sqrt{2}$. Since the numerical results of both velocities show oscillating convergence or divergence, the three-set GCI method was found inappropriate for this study. Thus, two-set GCI was employed for the spatial uncertainty calculation using fine and coarse grids. The details of this approach were given in a recent study [36]. The verification results are given below in Table 3 and 4.

One may see that the spatial uncertainty for the hover condition (0 knot) was about 6.5% and 3% for the headwind condition (40 knot).

Validation Study

Following the verification study, the numerical method should be validated with the available experimental data in the literature. The literature consists of experimental and numerical data [2,8]. The experimental results are of wind tunnel tests with and/or without helicopter fuselage. The numerical results are of an in-house developed code focused on helicopter rotor aerodynamics.

Validation of the numerical method was achieved for the hover condition at 293 RPM. The collective pitch angle

Table 4. Validation study at (M_{TIP} = 0.6).

Parameter	Experimental	HELIOS	Present study
c_T/σ	0.036	0.040	0.0347
c_Q/σ	0.0026	0.0029	0.0039
FM	0.493	0.517	0.3068

of the rotor blades is 5^0 at 75% blade section (the section that twist becomes zero). This condition corresponds to the experimental tip Mach number (M_{TIP} = 0.6) as indicated in the literature [2,8].

The results were compared with the experimental and in-house developed code results. One may see that there are discrepancies between experimental and numerical results, however, the results were found in good agreement. The non-dimensional thrust coefficient, torque coefficient and figure of merit (FM) parameters were compared, thus the FM appears to be far from other results. The difference in the FM was caused by the difference in the torque coefficient.

Rotor Aerodynamics

Several rotor parameters affect the efficiency of a helicopter's performance such as sweep angle, taper ratio, airfoil and chord distributions twist angle and rotation speed [18]. In the present study, only the effect of rotor speed was considered for hovering condition. Free rotor aerodynamics was investigated numerically for hover and headwind conditions. The free stream velocity was considered as 0 knot to simulate the hover condition [9]. In hover condition, total thrust and torque values were obtained at different rotor load conditions. Figure 5 shows the iso-value of velocity magnitude at Q = 25 as an arbitrary threshold.

Here, Q criterion was used as a vortex identification criterion applicable in incompressible flows and $Q > 0$ means that the vorticity magnitude is greater than the rate of strain [37–39]. Figure 5 shows the trend of thrust versus torque value for different blade loadings. The images show isosurfaces of the Q-criterion colored by velocity. Downstream of the blades, only tip vortices are seen. Due to insufficient computational capability, the wake that must continue axially downward from the rotor blade cannot be seen. This may also be due to the insufficient number of revolution of the rotor because it was revealed by [15] that as the number of revolution increases the wake distributions can be obtained clearly from the rotor center to the point that is one rotor diameter below. Another reason for not observing the swirling flow under the rotor blades is the grid structure. A detailed explanation was made in the study of [13]. As stated in this study, with the rotor running, the root vortex wake extends with the appropriate grid structure and number. In the present study, because of the computational cost, the solver time and total grid number were reduced. Accordingly, only a little vortex behind the rotor blades and some swirling structures were observed around the hub.

The vorticity around the rotor hub increases with the increase in the rotor loading. In addition, the vortices in the vicinity of blade trailing edges come closer to the middle of each blade. However, the tip vortices do not show any change with the rotational velocity. Figure 5 shows the iso-value of velocity magnitude at headwind condition. The vortex core in the hub shows a similar trend to the hover condition case. In this case, the loading has more effect on the trailing edge vortices and vortex splits are more visible. Thus, for the headwind condition, the full load condition (293 rpm) shows a dramatic difference when compared with lower blade loadings.
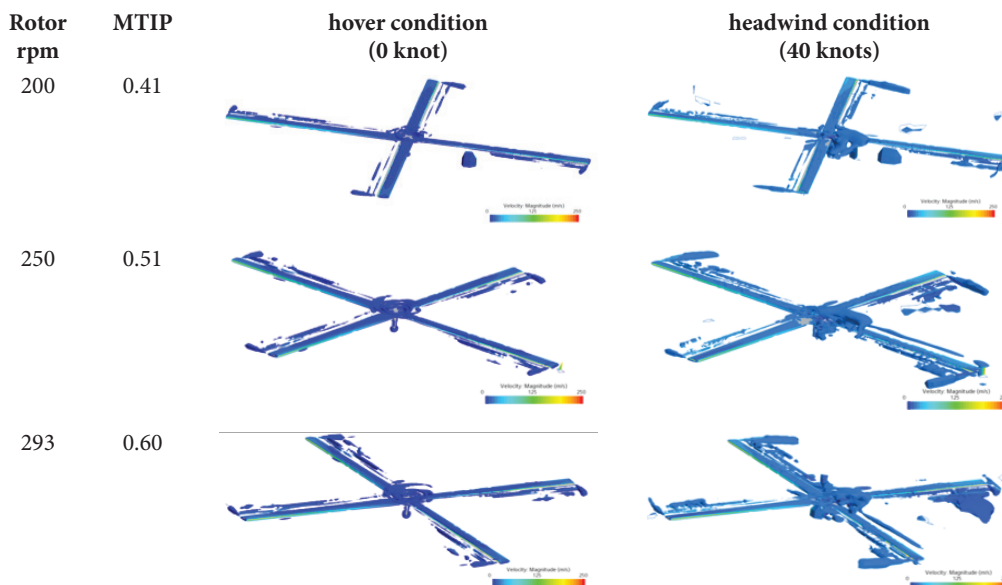
Rotor rpm	MTIP	hover condition (0 knot)	headwind condition (40 knots)
200	0.41		
250	0.51		
293	0.60		

Figure 5. Iso-values of velocity magnitude (Q=25) for hover and headwind conditions.

Figure 6 gives the relation between thrust (C_T) and torque coefficients (C_Q). The coefficients were calculated by the following equations.

$$C_T = \frac{T}{\rho(\Omega)^2 D^4} \qquad (5)$$

$$C_Q = \frac{Q}{\rho(\Omega)^2 D^5} \qquad (6)$$

Here, *T* is the total thrust force, *Q* is the torque, Ω is the blade rotational velocity (rpm) and *D* is the rotor diameter. Figure 6 presents the coefficients by dividing to the rotor solidity (σ). The vertical axis on the left corresponds to the hover condition (0 knot) while the vertical axis on the right

stands for the headwind condition (at 40 knots). At hover condition, considering that ground effects were neglected, the torque coefficients almost never change with the thrust coefficient. At headwind condition, there is not a linear relation between these two coefficients.

To see the effect of free stream velocity on the total thrust, non-dimensional thrust coefficients were obtained at each rotor velocity and condition. In Figure 7, the hover condition represents the lowest free stream velocity and it has nearly no effect on the thrust coefficient. The thrust coefficient for the headwind condition shows a decreasing behavior with the rotor velocity.

Figure 8 shows the effect of free stream velocity on the torque coefficient. One may see that the torque performance
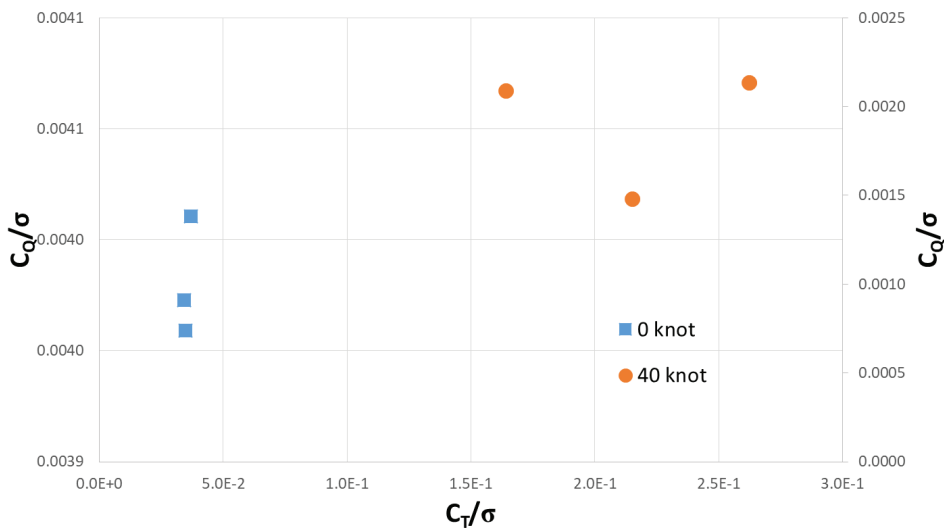

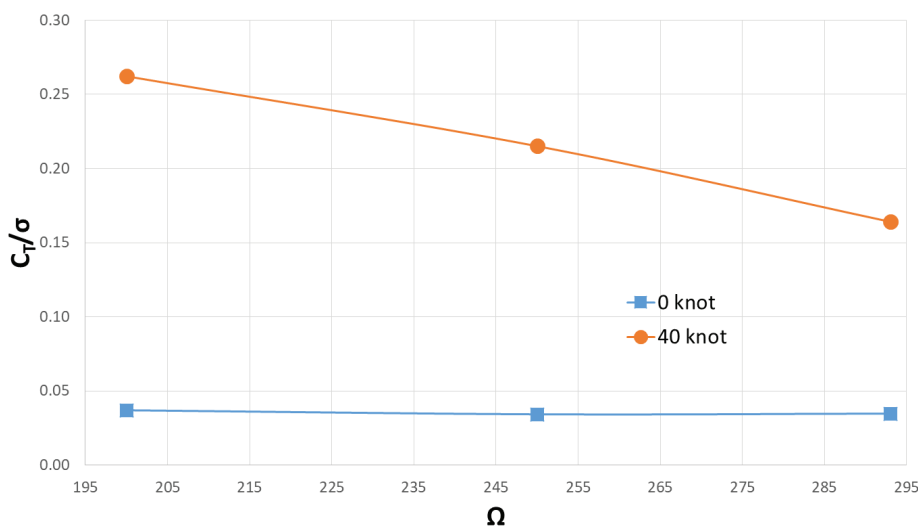**Figure 6.** Torque coefficient versus thrust coefficient for both cases.

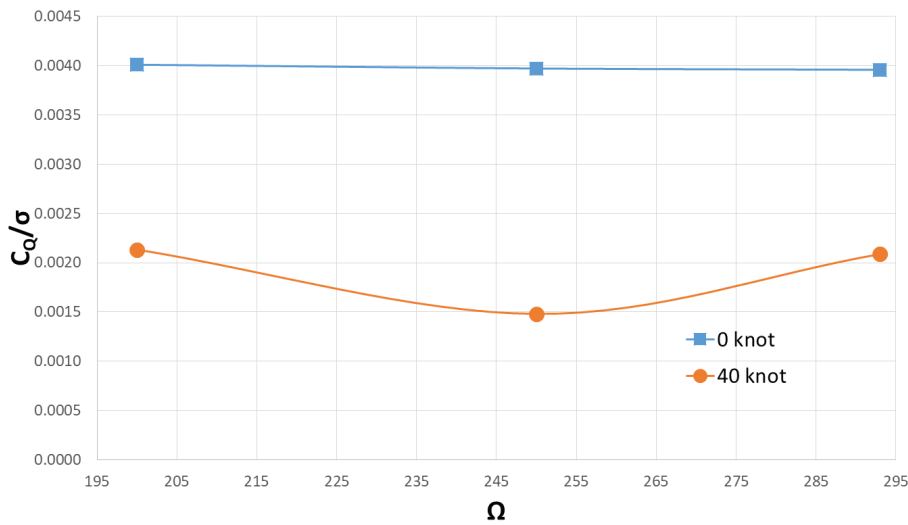**Figure 7.** Thrust coefficient – rotor velocity.

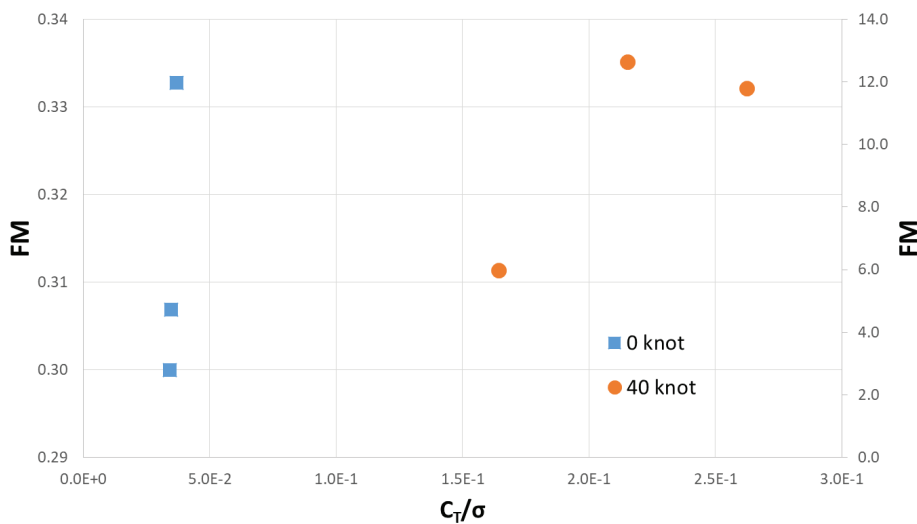**Figure 8.** Torque coefficient – rotor velocity.

Figure 9. Figure of merit – thrust coefficient.

was not affected by the free stream velocity at hover condition while there is little change at headwind condition.

In Figure 9, the figure of merit was given at each thrust coefficient for both free stream velocity conditions. The figure of merit was calculated by the following equation.

$$FM = \frac{1}{\sqrt{2}} \frac{C_T^{3/2}}{C_Q} \qquad (7)$$

The left axis is of hover condition and the right axis is of headwind condition. As expected, the figure of merit increases significantly with the increase in flow velocity. There is not a linear relation between the thrust coefficient and figure of merit. The highest value is obtained at lowest rotational speed for hover condition. However, in headwind condition, there is not a similar trend.

CONCLUSION

In this study, numerical analyses were conducted to investigate the effect of free stream velocity on rotor aerodynamics. For this purpose, Sikorsky S-76 main rotor was modeled and analyzed. The numerical approach was verified using the GCI method in terms of spatial uncertainty considering the scalar function is the thrust coefficient. Following this, the numerical approach was also validated by comparing the non-dimensional parameters with the available experimental data. The validation study was conducted for the main rotor at hover and headwind flow conditions and at maximum rotor rotational velocity (293 *RPM*) which corresponds to $M_{TIP} = 0.6$ to mimic the experimental conditions. After verification and validation study, the analyses were extended to different rotor rotational

velocities. It was concluded that the relation between thrust and torque coefficients show difference with the flow velocity and rotational velocity. As a final comparison, figure of merit was calculated at each scenario. In hover condition, both thrust and torque coefficients show little change at different rotor velocities. For this reason, the collective pitch angle comes to mind. For headwind condition, the thrust coefficient changes significantly while the torque coefficient changes little with the rotor velocity.

In addition to the numerical results, vortex structure was investigated at each case. However, due to low blade loadings, some minor trailing vortices were observed, and a swirling wake region was kept around the rotor hub. It is concluded that the mesh number and mesh resolution have a significant effect on this kind of vortex identification using a constant Q criterion. It is found that the vortex structure shows different behavior at different points of the rotor geometry. The hub vortex core shows a significant change with the increase in blade loading. The tip vortices occur for all loading and free stream velocities. However, it does not show any change with the blade loading and the vortex structure behind the blade trailing edge moves in the tip-hub direction, so the vortex separations become visible.

Future works on rotor aerodynamics operating behind a ship's flight deck are planned to investigate the ship airwake considering the ship-rotor interactions.

NOMENCLATURE

c	local chord (m)
c_T	rotor thrust coefficient
c_Q	rotor torque coefficient
FM	figure of merit
N_b	number of blades
Q	rotor torque (Nm)
R	blade radius (m)
T	rotor thrust (N)
U_N	numerical uncertainty
ρ	density (kg/m^3)
σ	rotor solidity
Ω	rotor rotational speed (rad/s)
M_{TIP}	blade tip Mach number

Abbreviation

URANS	Unsteady Reynolds-Averaged Navier-Stokes
SST	Shear Stress Transport
RBM	Rigid Body Motion
GCI	Grid Convergence Index
CFD	Computational Fluid Dynamics
CAD	Computer Aided Design
RPM	Rotation per minute
SA	Spalart-Allmaras
DES	Detached Eddy Simulation
PIV	Particle Image Velocimetry

REFERENCES

[1] Matías JC, Bardera R, Franchini S, Barroso E, Sor S. A comparative analysis of helicopter recovery maneuvers on a SFS by means of PIV and balance measurements. Ocean Eng 2023;275:114119. [CrossRef]

[2] Jain R. Hover predictions on the S-76 rotor with tip shape variation using helios. J Aircr 2018;55:66-77. [CrossRef]

[3] Wakefield NH, Newman SJ, Wilson PA. Helicopter flight around a ship's superstructure. Proc Inst Mech Eng Part G J Aerosp Eng 2002;216:13-28. [CrossRef]

[4] Lee RG, Zan SJ. Wind tunnel testing of a helicopter fuselage and rotor in a ship airwake. J Am Helicopter Soc 2005;50:326-337. [CrossRef]

[5] Gregorio FD, Pengel K, Kindler K. Industrial measurement campaign on fully equipped helicopter model, 15th Int. Symp. on Applications of Laser Techniques to Fluid Mechanics, Lisbon, Portugal: 2010.

[6] Barakos GN, Crozon C, Steijl R. Numerical Study of Shipborne Rotors, Tianjin, China: 2013, p. 1-28.

[7] Crozon C, Steijl R, Barakos GN. Numerical study of helicopter rotors in a ship airwake. J Aircr 2014;51:1813-1832. [CrossRef]

[8] Jain RK, Potsdam MA. Hover Predictions on the Sikorsky S-76 Rotor using Helios. 52nd Aerosp. Sci. Meet., National Harbor, Maryland: American Institute of Aeronautics and Astronautics; 13-17 January 2014, National Harbor, Maryland, 2014. [CrossRef]

[9]   Orbay E. Computational Fluid Dynamics Simulations of Ship Airwake with a Hovering Helicopter Rotor. (master thesis). METU, 2016.

[10]   Perera G, Jagathsinghe HDH, Dilshan SKK, Sudaraka MAM, Rangajeeva SLMD. Helicopter Main Rotor aerodynamic simulation with CFD. 9th Int. Res. Conf., Sri Lanka: 2016.

[11]   Shi Y, Xu Y, Zong K, Xu G. An investigation of coupling ship/rotor flowfield using steady and unsteady rotor methods. Eng Appl Comput Fluid Mech 2017;11:417-434. [CrossRef]

[12]   Şahbaz M, Sezer-Uzol N, Kurtuluş DF. Computational Analysis of A Model Scale Model Helicopter Rotor in Ground Effect. 9th Ank. Int. Aerosp. Conf., METU, Ankara, Türkiye: 2017.

[13]   Abras JN, Hariharan N. Comparison of Computational Fluid Dynamics Hover Predictions on the S-76 Rotor. J Aircr 2018;55:12-22. [CrossRef]

[14]   Tan JF, Zhou TY, Sun YM, Barakos GN. Numerical investigation of the aerodynamic interaction between a tiltrotor and a tandem rotor during shipboard operations. Aerosp Sci Technol 2019;87:62-72. [CrossRef]

[15]   Kara K, Brazell MJ, Kirby AC, Mavriplis DJ, Duque EP. Hover Predictions Using a High-Order Discontinuous Galerkin Off-Body Discretization. AIAA Scitech 2020 Forum, American Institute of Aeronautics and Astronautics; 2020. [CrossRef]

[16]   Barakos GN, Fitzgibbon T, Kusyumov AN, Kusyumov SA, Mikhailov SA. CFD simulation of helicopter rotor flow based on unsteady actuator disk model. Chin J Aeronaut 2020;33:2313-2328. [CrossRef]

[17]   Bardera R, Matias-Garcia JC, Garcia-Magariño A. PIV helicopter rotor-ground and rotor-frigate interaction study, American Institute of Aeronautics and Astronautics. AIAA AVIATION 2020 FORUM, June 15-19, 2020. [CrossRef]

[18]   İbaçoğlu H, Arikoğlu A. Multidisciplinary conceptual design methodology and design tool for rotor blades of advanced helicopters. J Aeronaut Space Technol 2022;15:19-33.

[19]   Ashok S, Rauleder J; Georgia Institute of Technology. NATO Generic Destroyer Moving-Ship Airwake Validation and Rotor-Ship Dynamic Interface Computations using Immersed Boundary Lattice-Boltzmann Method. Proc. Vert. Flight Soc. 79th Annu. Forum, West Palm Beach, Florida USA: The Vertical Flight Society; 2023, p. 1-21. [CrossRef]

[20]   Fernandez N, Owen I, White M, Wall A, Lee R, Yuan W, et al. Helicopter Aerodynamic Loading in the Airwake of a Moving Ship. Proc. Vert. Flight Soc. 79th Annu. Forum, West Palm Beach, Florida USA: The Vertical Flight Society; 2023, p. 1-11. [CrossRef]

[21]   Yu P, Hu Z, Hu J, Xu G, Shi Y. Numerical studies on the aeroelasticity of a shipboard helicopter rotor during engagement and disengagement with ship motions using CFD/CSD coupling approach. Aerosp Sci Technol 2023;141:108559. [CrossRef]

[22]   Zamiri A, Chung JT. Numerical evaluation of wind direction effects on the turbulence aerodynamics of a ship airwake. Ocean Eng 2023;284:115104. [CrossRef]

[23]   Jepson D, Moffitt R, Hilzinger K, Bissell J. Analysis and Correlation of Test Data From an Advanced Technology Rotor System. Contractor Report. NASA: USA; 1983.

[24]   White F. Fluid Mechanics. 8th edition. New York, NY: McGraw Hill; 2015.

[25]   Cengel Y, Cimbala J. Fluid Mechanics: Fundamentals and Applications. 4th ed. New York, NY: McGraw Hill; 2017.

[26]   Wilcox DC. Turbulence Modeling for CFD. 3rd edition. La Cañada, California, USA: DCW Industries; 2006.

[27]   Wilcox DC. Formulation of the k-w Turbulence Model Revisited. AIAA J 2008;46:2823-2838. [CrossRef]

[28]   Dogrul A. Numerical Prediction of Scale Effects on The Propulsion Performance of JOUBERT BB2 Submarine. Brodogr Teor Praksa Brodogr Pomor Teh 2022;73:17-42.

[29]   Sezen S, Delen C, Dogrul A, Atlar M. An investigation of scale effects on the self-propulsion characteristics of a submarine. Appl Ocean Res 2021;113:102728. [CrossRef]

[30]   Richardson LF. The Approximate Arithmetical Solution by Finite Differences of Physical Problems Involving Differential Equations, with an Application to the Stresses in a Masonry Dam. Philos Trans R Soc Lond Ser Contain Pap Math Phys Character 1911;210:307-357. [CrossRef]

[31]   Celik IB, Ghia U, Roache PJ, Freitas CJ, Raad PE. Procedure for Estimation and Reporting of Uncertainty Due to Discretization in CFD Applications. J Fluids Eng 2008;130. [CrossRef]

[32]   Praveen B, Vijayakumar R, Singh SN, Seshadri V. Flow characteristics on helodeck of a generic frigate ship model through experiment and CFD. Ocean Eng 2022;250:110912. [CrossRef]

[33]   Sarı S, Doğrul A, Bayraktar S. On The Computational Aerodynamics of a Generic Frigate, Istanbul, Türkiye: 2021, p. 397-403.

[34]   Cosner R, Oberkampf B, Rumsey C, Rahaim C, Shih T. AIAA Committee on Standards for Computational Fluid Dynamics: Status and Plans. 44th AIAA Aerosp Sci Meet Exhib Reno Nevada, USA: American Institute of Aeronautics and Astronautics; 2006. [CrossRef]

[35]   Xing T, Stern F. Factors of Safety for Richardson Extrapolation. J Fluids Eng 2010;132. [CrossRef]

[36]   Bilir AÇ, Doğrul A, Vardar N. An Extensive Investigation of Flow Conditioners Inside A Fi-Fi Monitor. Brodogr Teor Praksa Brodogr Pomor Teh 2022;73:161-177. [CrossRef]

[37]   Epps B. Review of Vortex Identification Methods. 55th AIAA Aerosp. Sci. Meet., Grapevine, Texas, USA: American Institute of Aeronautics and Astronautics; 2017. [CrossRef]

[38] Hunt JCR, Wray AA, Moin P. Eddies, stream, and convergence zones in turbulent flows. Cent. Turbul. Res. Proc. Summer Program, 1988, p. 193-208.

[39] Kolář V. Vortex identification: New requirements and limitations. Int J Heat Fluid Flow 2007;28:638-652. [CrossRef]